

Single-atom Ni-N₄ sites coordinate dual nonradical oxidation pathways via peroxyomonosulfate activation: Computational insights and in situ spectroscopic analyses

Qingming Zeng ^a, Yanjun Wen ^a, Xiaoguang Duan ^{b,*}, Xing Xu ^c, Jing Tan ^a, Qingyan Zhang ^a, Yilin Liu ^a, Qingyi Zeng ^{a,*}

^a School of Resources & Environment and Safety Engineering, University of South China, Hengyang, Hunan 421001, China

^b School of Chemical Engineering, The University of Adelaide, Adelaide SA5005, Australia

^c Shandong Key Laboratory of Water Pollution Control and Resource Reuse, School of Environmental Science and Engineering, Shandong University, Qingdao 266237, China



ARTICLE INFO

Keywords:

Nonradical oxidation
Ni-N₄
Peroxyomonosulfate
Charge transfer process
High-valent Ni species

ABSTRACT

In this work, we revealed a dual-pathway nonradical oxidation (NRO) system catalyzed by Ni single atom catalyst (NiN_4) accommodated in the carbon nitride substrate. The monatomic Ni coordinated with four N atoms (Ni-N_4) is determined as the dynamic catalytic center for peroxyomonosulfate (PMS) activation, showing an exceptional specific rate constant of $3.34 \text{ min}^{-1} \text{ g}^{-2} \text{ L}^{-2}$ (29.7 times that of CN/PMS system) in oxidizing bisphenol A and other refractory organics. In situ Raman, X-ray absorption, and electrochemical analyses as well as theoretical simulations demonstrate that the Ni-N_4 sites exhibit strong interaction with PMS benefited from the modulated electronic structures, resulting in nonradical surface-bonding active complexes ($\text{NiN}_4\text{-PMS}^*$) and deuterogenic high-valent Ni(IV)-Oxo species. The dual-pathway NRO process will spontaneously coordinate both electron transfer process via CN matrix and direct electron transfer by Ni(IV)-Oxo for selective organic oxidation with excellent anti-interference ability and adaptability.

1. Introduction

The release of persistent organic pollutants (POPs) into the environment, such as dyes, medicines, and phenolic compounds, has sparked widespread concern owing to their hazardous effects on the ecosystem [1–3]. Advanced oxidation processes (AOPs) based on peroxyomonosulfate (PMS) activation are defined as powerful remediation technologies to remove POPs from water owing to the high redox potential of the generated radicals [4,5]. Among the various PMS activation methods, heterogeneous activation via the radical pathway demonstrates notable efficacy and flexibility, offering energy efficiency and readily accessible attributes [5,6]. However, the complex water matrix poses great challenges to the radical pathway because it is easily affected by natural organic matters and other ions, resulting in a strong restriction on the oxidation of target contaminants [7,8]. Additionally, the widely existed halogen ions may be oxidized to halogen radicals to produce more toxic organic halides, [9,10] which may hinder the development of PMS-based AOPs.

In addition to typical radical pathway, other nonradical pathways (nonradical oxidation, NRO), e.g., singlet oxygen (${}^1\text{O}_2$), [11] electron transfer process (ETP), [12,13] and high-valent metal species [14,15] have been reported in heterogenous PMS activation systems. Among them, ${}^1\text{O}_2$ suffers from relatively short lifetime ($2.5 \times 10^{-6} \text{ s}$ in water), [16] which reduces the utilization rate of oxidants and hinders its efficacy in real application. Metastable intermediates (catalyst-PMS*), as typical oxidative species in ETP, and high-valent metal species are promising candidates for water remediation, owing to their much longer lifetime (e.g., minutes to days for catalyst-PMS*, and 7–10 s for Fe (IV)-Oxo), higher steady-state concentrations ($\sim 10^{-4}$ for $\sim 10^{-9}$ for catalyst-PMS*, Fe(IV)-Oxo $\gg 10^{-12} - 10^{-15} \text{ M}$ for radicals), ultrahigh utilization efficiency of oxidant, and selective reactivity toward organics. [12–15,17] Additionally, NRO can be conducted on the catalyst surface, deriving direct oxidation of organics with electron rich moieties without extra oxidizer consumption and radicals generation. [18] Furthermore, the generation of halogenated-free radicals is inhibited in NRO due to their moderate oxidation potential and specific reaction

* Corresponding authors.

E-mail addresses: xiaoguang.duan@adelaide.edu.au (X. Duan), qingyizeng@usc.edu.cn (Q. Zeng).

pathways, which minimizes the generation of halide disinfection intermediates.^[19] Therefore, developing suitable catalyst to selectively activate PMS via NRO would be essential to promote the PMS-based water purification.

Due to the high atomic efficiency, unique electronic structure and remarkable catalytic activity, single-atom catalysts (SACs) have rapidly become a research hotspot in environmental remediation, especially in Fenton-like AOPs.^[20,21] In N-rich carbon material, the electron-rich N dopants can create Lewis basic sites, which are prone to combine with the transition metal atoms (M, Lewis acid) to form a strong M-N_x coordination.^[5] Graphitic carbon nitride (CN) is a special N-doped graphene framework composed of s-triazine or tri-s-triazine structural motives with sp²-C and sp²-N atoms, which is an ideal substrate for coordinating single-metal atoms by embedding into the nitrogen-rich “sixfold cavities” to form M-N_x sites.^[22] The coordinated M-N_x sites always act as the reactive centers for PMS adsorption and activation in both radical and nonradical pathways. Specifically, a CN supported Mn-N₄ sites facilitated PMS activation via the cleavage of the O-O bond into high valent Mn(IV)-oxo species for p-chlorophenol oxidation.^[21] Zhang et al. reported CN supported Fe-N₄ sites played the most important roles for ¹O₂ generation with 100% selectivity.^[20] Jiang et al. discovered that CN based Co-N₄ sites facilitates the formation of Co (IV)=Oxo species by PMS activation.^[14] A Fe(III) doped CN was reported to activate PMS under a high-valent iron-oxo species as the dominant reactive species for p-chlorophenol oxidation.^[23] However, the mechanism of the nonradical activation pathway of PMS by CN-based SACs remains largely unexplored, and dual-pathway NRO based organic selective degradation was rarely reported.

In this work, a CN based Ni SAC (NiN₄) with tunable Ni loading amount was prepared by a scalable thermopolymerization and applied to activating PMS for organic oxidation in water remediation. The monodispersed Ni atom on the CN was bonded with four N atoms (Ni-N₄) and conferred highly modulated electronic structures, which exhibited strong interaction with PMS and derived a novel dual-pathway NRO process for highly efficient water remediation with selective oxidation of organic contaminants. The performance and mechanism of the NiN₄/PMS system toward wide range of POPs, including dyes, BTEX, antibiotics and phenols, was systematically revealed through series of experiments. Electrochemical tests and theoretical computations were conducted to comprehensively elucidate selective oxidation of organics in the NiN₄/PMS system. The results deepened the understanding of PMS activation by CN-based SACs in a dual-pathway NRO mechanism and paved the way to develop highly selective Fenton-like systems for POPs degradation toward water remediation.

2. Experimental section

2.1. Chemical reagents list and catalyst synthesis

Urea (99%), bisphenol A (BPA, 99%), humic acid (HA, ≥90%), sodium bicarbonate (NaHCO₃, ≥99.8%), sodium dihydrogen phosphate (NaH₂PO₄, 99%), peroxyomonosulfate (PMS, >47%), nickel oxide (NiO, 99%), nickel nitrate (Ni(NO₃)₂, ≥ 98%), nickel powder (Ni, 99.5%), 5,5-dimethyl-1-pyrroline N-oxide (DMPO, 97%) and 2,2,6,6-tetramethyl-4-piperidinol (TEMP, 98%), ethanol (EtOH, ≥99.5%) , D₂O (99%), oxalate (≥99%), EDTA-Na₂ (EDTA, ≥99%), dimethylsulfoxide (DMSO, ≥98%), methyl phenyl sulfoxide (PMSO, ≥98%), Phenol (PhOH, ≥99%), methylene blue (MB, 96%), methyl orange (MO, 96%), Rhodamine B (RhB, 99%), tetracycline hydrochloride (TET, 96%), ibuprofen (IBU, 98.0%), p-nitrophenol (PNP, 99.7%), atrazine (ATZ, 97.0%), aureomycin hydrochloride (CTC, ≥80%), oxytetracycline hydrochloride (OTC, 95%), tert-butyl alcohol (TBA, 99%), Furfuryl alcohol (FFA, ≥99.8%), p-benzoquinone (P-BQ, 99%) were obtained from Shanghai Aladdin Biochemical Technology Co., Ltd. (Shanghai, China).

Carbon nitride polymer (CN) was prepared by a facile annealing process. Briefly, 20 g urea was milled for 1 h in a mortar, and then

transferred into a ceramic crucible. After annealing at 450 °C for 4 h with a heating rate of 5 °C/min in a muffle furnace, the powder CN was obtained. The NiN₄ was synthesized following the same procedure except the mixture of 0.3 g nickel nitrate with 20 g urea, denoted as NiN₄-3 for comparison. Additionally, the samples prepared by adding 0.1 g, 0.2 g, and 0.4 g nickel nitrate (denoted as NiN₄-1, NiN₄-2 and NiN₄-4, respectively), and NiO-CN and Ni₂O₃-CN (replacing nickel nitrate with 0.3 g nickel oxide or 0.3 g nickel trioxide) were also prepared for comparison. The detailed characterizations of the as prepared samples were supplemented in the [Supplementary Material \(Text S1 and S2\)](#).

2.2. Experimental operation details

49.5 mL contaminant solution with a concentration of 20 mg L⁻¹ was added to a beaker with a capacity of 100 mL and stirred in a thermostat water bath with magnetic stirring. The temperature of the thermostat water bath was maintained at 30 ± 1 °C. The initial PH of BPA solution is about 5.6, and 0.1 M sodium hydroxide (NaOH) or hydrochloric acid (HCl) is used to adjust the PH if necessary. In general, 0.01 g NiN₄ catalyst was added into the beaker and stirred continuously for ten minutes to achieve the adsorption/desorption balance, then 0.5 mL of 200 mM PMS solution was added, continued stirring and sampling within a given time interval, 1.0 mL of the reaction solution was collected and filtered through a 0.44 μm millipore film, and then, it was injected into a vial for further analysis. The radical scavenging experiment and stability experiment were performed with the same steps. EtOH, FFA, TBA, p-BQ were added for radical scavenging experiment. For the replicate experiments, the catalyst was recovered firstly by filtration of the reaction solution using a 0.44 μm millimeter pore membrane, followed by elution of the catalyst on the membrane with ultrapure water, and then the aqueous solution obtained was filtrated again, so repeated for five times, finally, the catalyst was obtained after vacuum drying for reuse. The concentration of BPA was detected by a high-performance liquid chromatography (HPLC, Agilent 1260, USA), with the C-18 column at a wavelength of 225 nm (mobile phase was 70% methanol and 30% water, speed was 0.3 mL min⁻¹). All experiments were repeated three times, and average data were obtained as analysis data. Electron paramagnetic resonance (EPR) spectra of reactive oxygen species (ROS) in catalytic system were identified by a Bruker micro EPR spectrometer. The details of theoretical calculations were supplemented in the [Supplementary Material \(Text S3\)](#).

3. Results and discussion

3.1. Characterization of NiN₄ catalysts

The proposed NiN₄ catalyst was prepared via a simple one-step thermopolymerization under ambient condition using urea and nickel nitrate as precursors ([Fig. 1a](#)). After doping with Ni, the obtained NiN₄ catalyst exhibits a porous coral-like morphology with curled and folded edges ([Figs. 1b-1e](#) and [S1a-S1b](#)) when compared with the pristine CN (smooth sheet-like shape, [Figs. S1c-S1d](#)) as illustrated by the scanning electron microscope (SEM) and transmission electron microscopy (TEM) images. This coral-like morphology is beneficial for reactive substance transport and providing large accessible surface areas.^[24] Thus, Ni doping causes the in-plain strains and intertwined of two-dimensional (2-D) CN. Furthermore, no nanoparticles were observed in both TEM and high-resolution TEM (HRTEM) images ([Figs. 1d-1e](#)), indicating Ni species did not congregate during the annealing. Scanning TEM (STEM) image and energy dispersive spectrometer (EDS) mappings of NiN₄ indicate that the catalyst was composed of uniformly dispersed C, N and Ni elements ([Fig. 1f](#)). The amount of Ni was 3.2 wt% based on the inductively coupled plasma-mass spectrometry (ICP-MS) results ([Fig. S2](#)). The highly dispersed bright spots (highlighted by yellow circles) in the high-angle annular dark-field scanning TEM (HAADF-STEM)

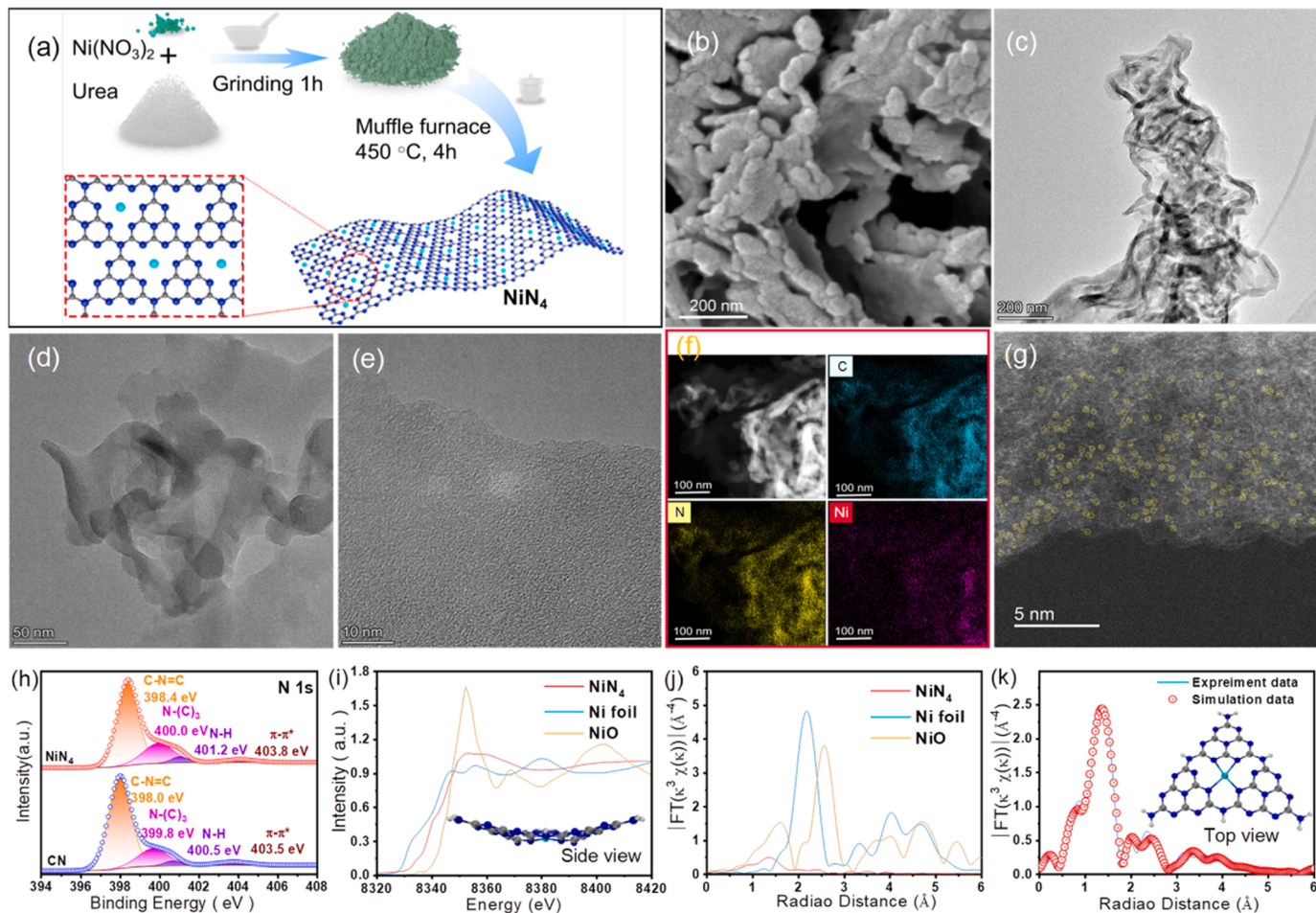


Fig. 1. (a) Schematic illustration of the synthesis process, (b) SEM image, (c, d) TEM images, (e) HRTEM image, (f) EDS mapping and (g) HAADF-STEM images of NiN₄; (h) N 1 s XPS spectra of NiN₄ and CN; (i) Normalized Ni K-edge XANES and (j) k^3 -weighted Fourier transform of NiN₄, Ni foil and NiO; (k) EXAFS fitting curve in R space (insets of i and k: optimized density functional theory (DFT) calculation model of NiN₄, Ni: cyan, N: blue, C: gray, H: white).

image (Fig. 1g) confirmed the single-atom state of Ni in the NiN₄. This atomic level doping of Ni did not change the crystal structure (Figs. S3), while only weakened the crystallinity of 2-D CN due to the crimpation. On the other hand, the wrinkled feature affords a larger specific surface area for NiN₄ (108.0 m²/g) compared to CN (87.5 m²/g) (Fig. S4 and Table S1), which could provide more active sites for heterogeneous catalysis.

The X-ray photoelectron spectroscopy (XPS) spectrum indicated that the NiN₄ consisted of Ni, N, and C elements (Fig. S5a). The high-resolution Ni 2p spectrum was convoluted into the typical peaks at 855.5 and 872.9 eV (Fig. S5b), matching well with Ni 2p_{3/2} and Ni 2p_{1/2} spectra.^[25] The Ni 2p_{3/2} at the low binding energy was located between metallic Ni (853.1 eV) and ionic Ni (856.0 eV) spectra, further confirmed the existence of scattered single atomic. Moreover, compared with CN, the N peaks in the NiN₄ showed a blue shift, which should be related to strong metal-support interactions via the coordination between N and Ni (Fig. 1h).^[26] However, the C 1 s spectra of NiN₄ and pure CN showed no significant difference (Fig. S5c), which indicated Ni atoms were not coordinated with C directly.^[27] The above results initially demonstrate that single atomic Ni was coordinated with the N atoms of the triazine ring in CN.

The X-ray absorption near-edge structure (XANES) of NiN₄ showcased that the absorption edge position of Ni single-atom was located between that of Ni foil and NiO (Fig. 1i), indicating the valence state of the Ni atom was between 0 and +2, and the coordination atoms for Ni sites should be those with a weaker electronegativity than O, such as C and N.^[20] The Fourier transform extended X-ray absorption fine

structure (FT-EXAFS) unveiled that NiN₄ exhibited a dominant peak at 1.4 Å (Fig. 1j), which was different from Ni-Ni and Ni-O, proving Ni exclusively coordinated with the N atoms in NiN₄.^[27] According to the curve fitting by EXAFS (Fig. 1k and Table S2), the coordination configuration of the Ni atom was determined to be Ni-N₄, and the specific coordination structure (inset of Fig. 1k) was determined by the localized orbital locator (LOL). As presented in Fig. S6, there were four N sites in the middle near the Ni site with the presence of localized electrons between Ni (red text N), which was the result of the specific coordination of N with Ni.^[27] Noteworthy, the optimized NiN₄ structure was distorted (inset of Fig. 1i), which was caused by Ni doping and coincided with the edge curl morphology (Figs. 1b-1d), because the coordination of Ni and N should make the electrons redistributed and break the original electronic balance, thus causing the structural distortion. Furthermore, the wavelet transform (WT) plot of NiN₄ showed the WT maximum at 5.5 Å⁻¹, which was associated with the Ni-N bond distinguishing from Ni foil and NiO (Fig. S7). Generally, these results further confirmed the atomically dispersed Ni sites and its coordination condition with four N atoms on the CN matrix.

3.2. Water purification performance of NiN₄/PMS system

The NiN₄ showed high activity in PMS activation for BPA degradation. As depicted in Fig. 2a, BPA was completely removed within 15 min in the NiN₄/PMS system with an observed rate constant (k_{obs}) of 0.41 min⁻¹, which is about ~29.7 times that of the CN/PMS system, demonstrating the activity was attributed to monatomic Ni-N₄ sites.

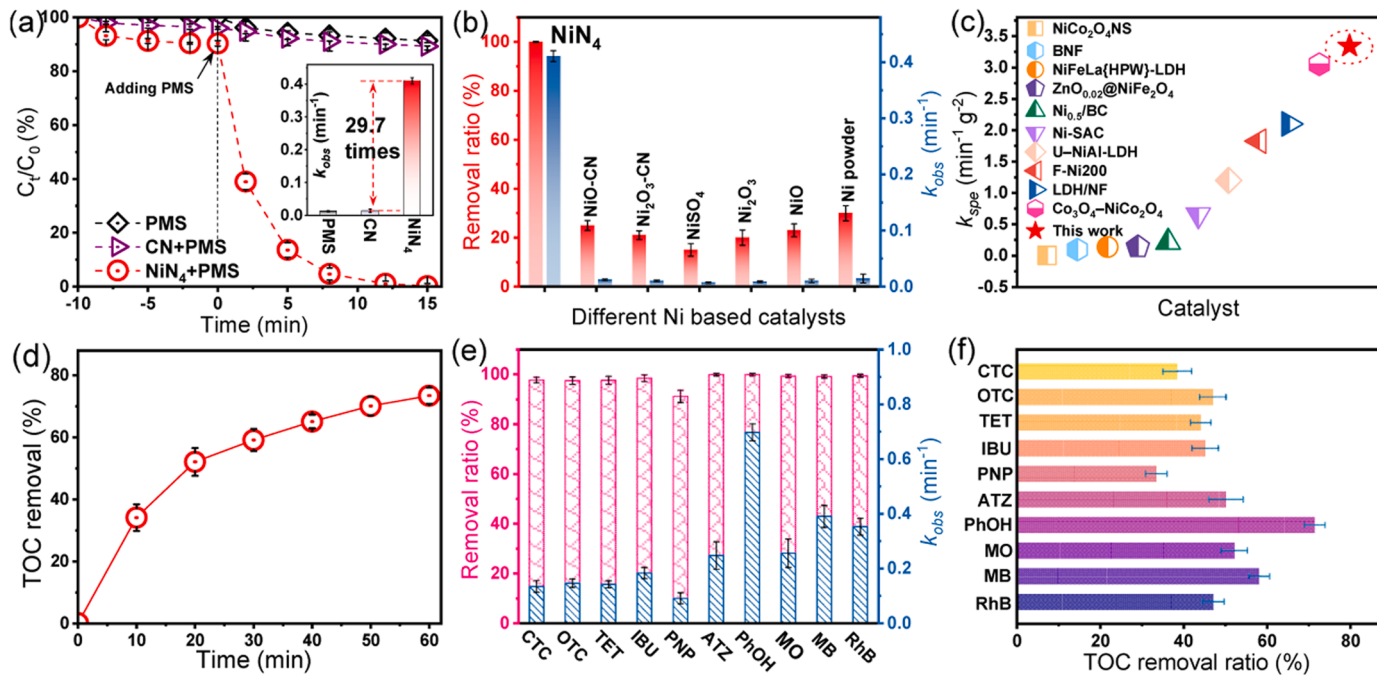


Fig. 2. BPA degradation in PMS activation system (a) under different conditions (inset: corresponding k values) and (b) using different Ni-based materials; (c) Comparison of specific rate constant (k_{sp}) value of NiN_4 and other reported Ni based catalysts (details and references can be found in Table S3). (d) TOC removal rate in the NiN_4 /PMS/BPA system; (e) Degradation efficiency and (f) TOC removal of various organic substances in NiN_4 /PMS system (60 min for CTC, OTC, TET, IBU and PNP, 5 min for PhOH, and 15 min for ATZ, MO, MB and RhB; 1 h for TOC results). Conditions: [catalyst] = 0.2 g L⁻¹, [oxidants] = 2 mM, [pollutant] = 20 mg L⁻¹, T = 30 °C, initial pH = 5.6.

Furthermore, its catalytic activity is much higher than other Ni species or clusters Ni (Fig. 2b). Compared with some reported Ni-based catalysts, the NiN_4 also exhibited the state-of-art value for PMS activation (Fig. 2c, Table S3). Notably, NiN_4 had a relatively higher adsorption effect of BPA (10% after 10 min) than CN (3%) in the adsorption phase (Fig. 2a), which could be ascribed to the increased specific surface area of NiN_4 (Table S1) and plentiful Ni-N_4 sites. In the NiN_4 /PMS system, BPA was effectively decomposed into small-molecule organics based on the results of ultra-high performance liquid chromatography mass spectrometry (UPLC-MS, Figs. S8 and S9) with a mineralization efficiency of 52% after 20 min and 73% after 60 min (Fig. 2d), indicating the highly oxidation capacity of the NiN_4 /PMS system. In addition, peroxyacetic acid (PAA), peroxydisulfate (PDS) and hydrogen peroxide (H_2O_2) could be also activated by NiN_4 for BPA degradation (Fig. S10), suggesting the outstanding catalytic activity of NiN_4 in Fenton-like AOPs.

In the control experiments, the effect of Ni amount was first investigated, which showed that the activity of NiN_4 was improved when increasing Ni amount from 1.1 ~ 3.2 wt% while slightly weakened with the amount of 5.6 wt% (Figs. S2 and S11). An optimized Ni amount was about 3.2 wt%, which is the sample (NiN_4) used in this study without specific notification. As to the reaction temperature, slight enhancement was exhibited when increasing the temperature (Fig. S12), suggesting that the atomic dispersion of Ni can realize the peak kinetics in the NiN_4 /PMS/BPA system. Moreover, in the range of initial pH from 3.1 to 10.0, BPA could be completely degraded within 15 min with the k values higher than 0.23 min^{-1} (Fig. S13a) and extremely low Ni leaching lower than 10 $\mu\text{g L}^{-1}$ (Fig. S13b), indicating that the NiN_4 /PMS system has high adaptability and stability in a wide pH range. Undoubtedly, increasing the dosage of NiN_4 or PMS caused considerable promotion to BPA degradation (Fig. S14), while the promotion effect became moderate when the PMS concentration is higher than 2 mM, due to the maximum utilization of all NiN_4 sites.

The presence of inorganic ions, such as H_2PO_4^- and HCO_3^- , showed slight suppression on the BPA degradation (Fig. S15), which could be

due to their complexation with the active metal sites on the catalyst. [20] However, NO_3^- had negligible effect on the activity of the NiN_4 /PMS system, while Cl^- showed positive effect on the BPA oxidation (Fig. S15), which should be attributed to interaction of Cl^- and PMS that contributed to the BPA degradation (Fig. S16). In the presence of humic acid (Fig. S17), the BPA degradation rate only decreased slightly along with the increasing concentration (0–200 mg L⁻¹), implying selective oxidation of BPA by the NiN_4 /PMS system. Besides, there was no significant change in the removal rate of BPA by NiN_4 /PMS system in different water backgrounds (Fig. S18), verifying a good interference immunity in practical water. Furthermore, after five cycles, the NiN_4 /PMS system still had a high activity with a removal ratio of 96.5% and virtually negligible Ni leaching (Fig. S19), and no obvious change was observed for the crystal structure of NiN_4 or the chemical states of C, N and Ni in used NiN_4 (Fig. S20), further demonstrating the high stability of NiN_4 catalyst.

To further reveal the possible selective oxidation of NiN_4 /PMS system, the degradation of some other refractory organic pollutants, including dyes (e.g., rhodamine B (RhB), methyl orange (MO) and methylene blue (MB)), typical BTEX (e.g., ibuprofen (IBU), p-nitrophenol (PNP) and phenol (PhOH)), antibiotics (e.g., chlortetracycline (CTC), tetracycline (TET) and oxytetracycline (OTC)), and triazine (e.g. atrazine (ATZ)), by the NiN_4 /PMS system were tested. The result indicated PhOH was completely degraded within 5 min with a k value of 0.7 min^{-1} (Fig. 2e), and ATZ, MO, MB and RhB were removed within 15 min with k values of 0.25, 0.26, 0.39 and 0.35 min^{-1} , respectively. However, CTC, OTC, TET, IBU were relatively tough and removed after 60 min with k values of 0.13, 0.15, 0.14 and 0.18 min^{-1} , respectively. The degradation of PNP was only 92.1% after 60 min with a k value of 0.09 min^{-1} . However, the adsorption of these organics was only around 10% (Fig. S21). After 60 min operation, the mineralization ratios of these refractory organic pollutants were also considerable with the value higher than 43% (except for 33.5% for PNP and 38.5% for CTC) (Fig. 2f). Besides, these TOC removal rates showed a roughly positive linear correlation with the $\ln(k_{\text{obs}})$ (Fig. S22). These results indicated that the

NiN_4/PMS system exhibited selective oxidation for different organics, while excellent activity was obtained for their degradation. In general, NiN_4/PMS system shows excellent catalytic performance and anti-interference ability, and thus may have good application prospects.

3.3. Reactive species detection in NiN_4/PMS system

The scavenging experiments indicates that ethanol (EtOH, scavenger for $\bullet\text{OH}$ and $\text{SO}_4^{\bullet-}$) and tert-butyl alcohol (TBA, scavenger for $\bullet\text{OH}$) only slightly inhibited BPA oxidation (Fig. 3a), while furfuryl alcohol (FFA, scavenger for $^1\text{O}_2$ and $\bullet\text{OH}$) exhibited considerable inhibition.[20] Additionally, the $\text{O}_2^{\bullet-}$ radical was also analyzed via scavenging test (Fig. S23), which excluded its contribution on BPA degradation. These results preliminary suggested a non-free radical pathway mechanism in the NiN_4/PMS system.[28] The existence of ROS in the NiN_4/PMS system was further verified by the electron paramagnetic resonance (EPR) analysis. Typical 2,2,6,6-tetramethylpiperidinyloxy (TEMPO)- $^1\text{O}_2$ adducts was detected and no obvious change was observed when adding BPA into the system (Fig. 3b), speculating $^1\text{O}_2$ had limited effect on BPA degradation.[29] Additionally, only neglectable signals of 5,5-Dimethyl-1-pyrroline N-Oxide (DMPO)- $\bullet\text{OH}$ and DMPO- $\text{SO}_4^{\bullet-}$ were

detected, while the signal of DMPO- $\text{O}_2^{\bullet-}$ was not observed (Fig. S24). To further reveal the contribution of $^1\text{O}_2$, D_2O was used to replace H_2O as the solvent to prolong the lifetime of $^1\text{O}_2$.[16] However, no significant enhancement was observed for the BPA degradation (Fig. 3c), further unveiling the negligible role of $^1\text{O}_2$ in NiN_4/PMS system. When removing dissolved O_2 by N_2 , no obvious change was observed for the degradation rate (Fig. S25), unveiling the dissolved O_2 was not involved in the BPA oxidation. However, increasing the premixing time of NiN_4 and PMS gradually inhibit the degradation efficiency of BPA (Fig. 3d) and the other organics (Fig. S26). If the interaction of NiN_4 and PMS causes the conversion of PMS, e.g., generation radicals or high-valent Ni species, the premix can cause the consumption of PMS and reduce the organic oxidation efficiency.[30] Combined with the consumption of PMS in the NiN_4/PMS system (Fig. S27), these results indicate the existence of strong interaction between NiN_4 and PMS with the conversion of PMS. Basically, the roles of radicals and $^1\text{O}_2$ were neglectable to BPA oxidation. Therefore, other pathways in the NiN_4/PMS system may co-existed and need to be identified.

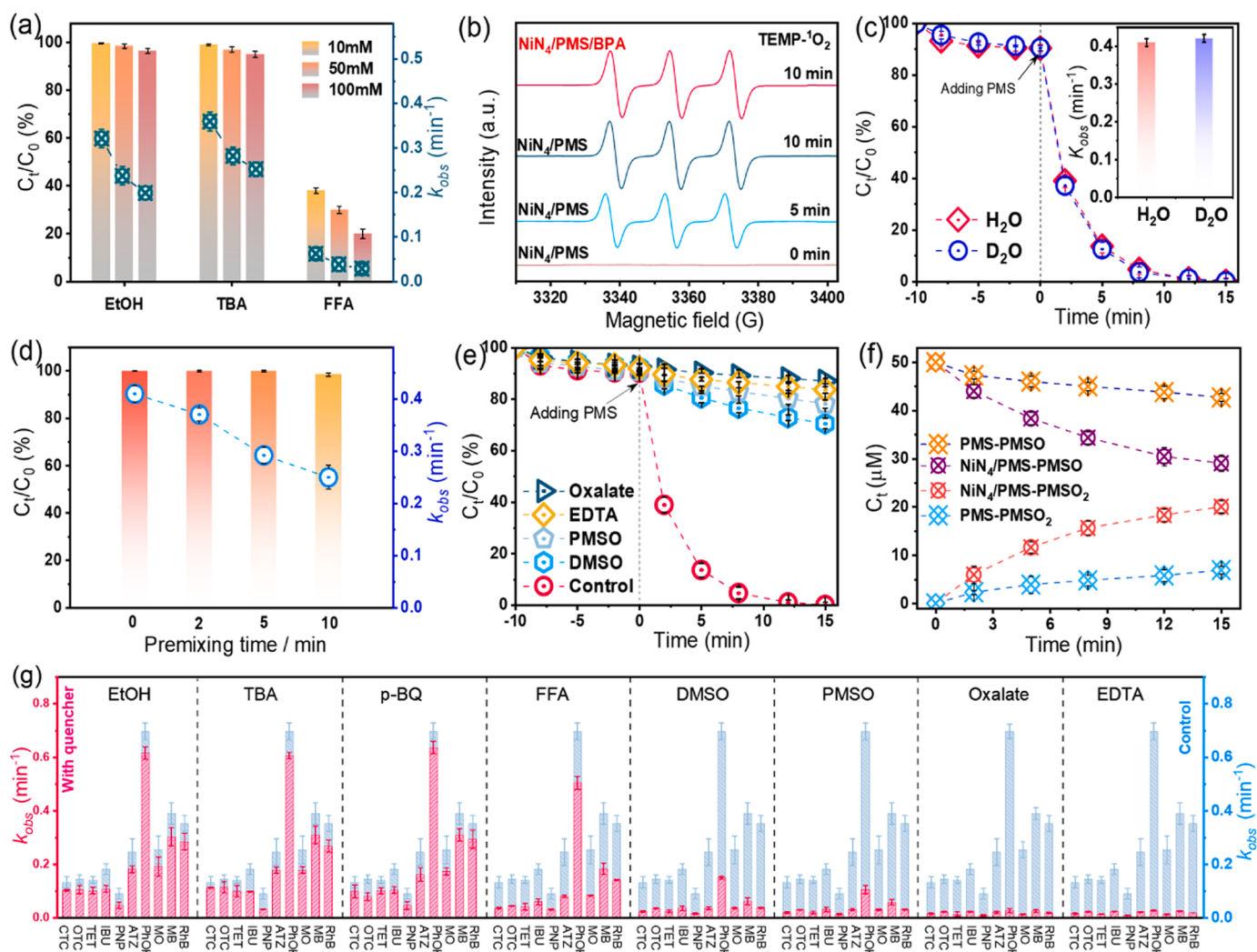


Fig. 3. (a) Scavenging experiments for BPA degradation by the NiN_4/PMS system; (b) EPR spectra of $^1\text{O}_2$ at different reaction times in different systems; (c) BPA degradation by the NiN_4/PMS system in H_2O and D_2O matrix; (d) Effect of premixing time of NiN_4 and PMS for BPA degradation; (e) Influence of DMSO (0.1 M), PMSO (0.1 M), oxalate (25 mM) and EDTA (1 mM) on BPA degradation; (f) PMSO and PMSO₂ concentrations at PMS (2 mM) and NiN_4/PMS system; (g) Scavenging experiments for different organics degradation by the NiN_4/PMS system. Conditions: [catalyst] = 0.2 g L^{-1} , [PMS] = 2 mM, [pollutant] = 20 mg L^{-1} , T = 30 °C, initial pH = 5.6.

3.4. High-valent Ni(IV)-Oxo species in NiN_4/PMS system

To further verify the essential role of Ni atom sites, oxalate and EDTA were used as chelators, which can form stable water-soluble chelates with the transition metals, allowing the Ni atom sites to be occupied and inactivated.[31]. The degradation of BPA was almost inhibited under the presence of these chelates (Fig. 3e). Therefore, Ni atom sites are the catalytic centers in the NiN_4/PMS system. Typically, transition metal catalytic sites can directly transfer electrons ($\text{M}^{n+}/\text{M}^{(n+1)+}$) with PMS to generate different radicals, e.g., $\bullet\text{OH}$, O_2^- and SO_4^{2-} , or ${}^1\text{O}_2$.[32,33] However, the above results excluded this speculation. In addition to these typical processes, other highly active process, such as generating high-valent metal-oxo species (e.g., $\equiv\text{Ni}(\text{IV})=\text{O}$), could also exist. To verify the generation of high-valent Ni(IV)-Oxo species, the specific

O-atom-transfer reaction from sulfoxides to sulfones was applied by using dimethylsulfoxide (DMSO) and methyl phenyl sulfoxide (PMSO) as reactive agents. Since DMSO/PMSO can be oxidized by high-valent Ni (IV)-Oxo species to produce the corresponding sulfone ($\text{DMSO}_2/\text{PMSO}_2$) via the oxygen transfer pathway, which is distinctly different from the radical-based oxidation pathway.[14,34] Under the presence of DMSO and PMSO, the removal rate of BPA was significantly inhibited and the removal ratios were only 29.5% and 21.8%, respectively (Fig. 3e). Furthermore, the PMSO consumption and PMSO_2 production in the NiN_4/PMS system were also investigated (Fig. 3f). Compared with the system with only PMS, the production of PMSO_2 was much higher in the NiN_4/PMS system (PMSO conversion efficiency, 40% vs 13%), further suggesting the formation of high-valent Ni(IV)-Oxo species.[34] In addition, the results of scavenging tests for different organics

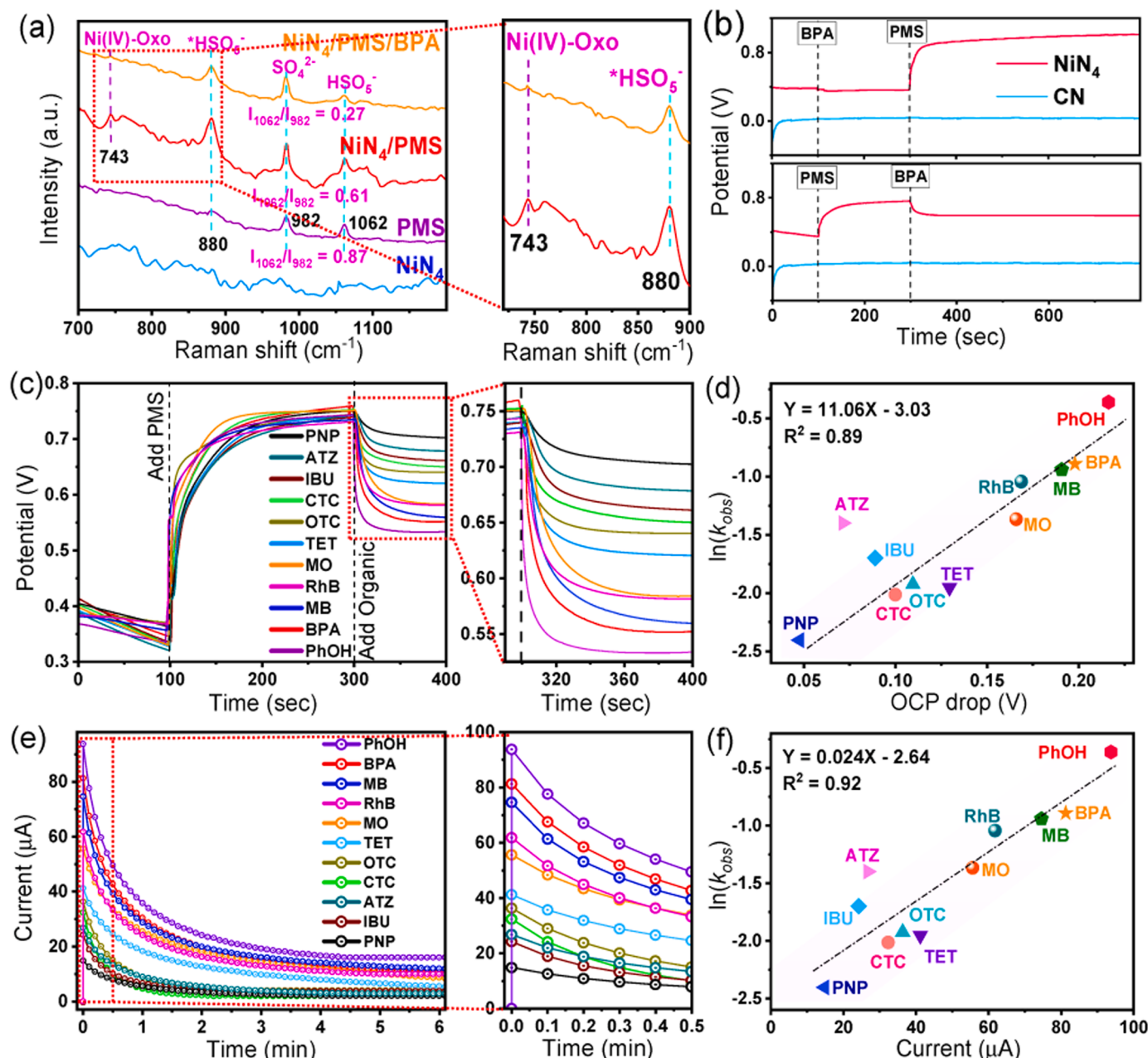


Fig. 4. (a) *In situ* Raman spectra; (b) OCP curves of the electrodes composed of CN or NiN_4 under the different sequence of adding PMS or BPA (0.1 M Na_2SO_4 as supporting electrolyte); (c) OCP curves of electrode composed of NiN_4 under the addition of different pollutants. (d) The relationship between the OCP drop and $\ln(K_{\text{obs}})$ of different organics. (e) Current flowing from PMS cell to the pollutant cell in GOS when adding different organics. Conditions: [PMS] = 2 mM, [pollutant] = 20 mg L⁻¹, T = 30 °C, initial pH = 5.6. The linear fitting in (d) and (f) was carried out by excluding ATZ.

degradation by the NiN₄/PMS system were also indicated similar phenomenon. As depicted in Fig. 3g, compared to the minor inhibition of organic degradation in the existence of EtOH, TBA, p-BQ, and FFA (although the inhibition by FFA was slightly greater), the presence of DMSO and PMSO inhibited the degradation of organics quite dramatically, further suggesting the dominance of high-valent Ni(IV)-Oxo species in the process of organic degradation in the NiN₄/PMS system.[23] In addition, the almost complete inhibition of the organic degradation by Oxalate and EDTA further suggests that the Ni atom sites is the active site of NiN₄. Therefore, high-valent Ni(IV)-Oxo species would be formed in the NiN₄/PMS system and predominate the organics degradation.

The interaction between NiN₄ and PMS for the formation of high-valent Ni(IV)-Oxo species was further revealed by in-situ Raman and XANES. As shown in Fig. 4a, the interaction of NiN₄ and PMS caused an obviously new peak at ~880 cm⁻¹, corresponding to the adsorbed PMS molecules on NiN₄ to form a metastable PMS adsorption species (*HSO₅⁻, NiN₄-PMS*).[21] Additionally, the Raman peak intensity ratio (I₁₀₆₂/I₉₈₂) of 1062 cm⁻¹ (HSO₅⁻) to 982 cm⁻¹ (SO₄²⁻) decreased from 0.87 to 0.61, indicating the decomposition of PMS to form SO₄²⁻. At the position of 743 cm⁻¹, a new Raman peak appeared, although the intensity of this peak (743 cm⁻¹) was weak due to the low Ni contents in NiN₄, the Raman observation was in situ, and the disparity among the Raman spectra was sufficient to identify the presence and the absence of such a peak, thus verifying the existence of the Ni(IV)-Oxo species in the NiN₄/PMS system[21]. This result indicates that PMS molecules will bond with the Ni-N₄ site and cause the dissociation and transformation into SO₄²⁻ and Ni(IV)-Oxo species.[35] After adding BPA, the peak at 743 cm⁻¹ was significantly reduced immediately (Fig. 4a), thus implying the rapid interaction between BPA and Ni(IV)-Oxo species, and also suggesting that Ni(IV)-Oxo species are highly oxidative to trigger a direct electron transfer from BPA to Ni(IV)-Oxo. Meanwhile, the peak at 880 cm⁻¹ was also decreased, indicating BPA also consumed NiN₄-PMS* species via a possible electron transfer process. Furthermore, the value of I₁₀₆₂/I₉₈₂ further decrease to 0.27, which should be ascribed to the oxidation of BPA facilitated the dissociation of PMS on the NiN₄. The XANES results indicated that the adsorption curve of NiN₄ showed positive shift in the presence of PMS (Fig. S28), which could be attributed to the formation of Ni(IV)-Oxo species. And the decreased occupation of outermost electron orbits in Ni(IV)-Oxo species caused a slightly enhanced intensity of the white line peak, demonstrating a more oxidized Ni valence state.[36] Generally, these results collectively verify the existence of Ni(IV)-Oxo species in the NiN₄/PMS system.

3.5. Electron-transfer process in NiN₄/PMS system

In addition to the formation of Ni(IV)-Oxo species, nonradical processes, e.g., electron-transfer process (ETP),[13] would be also existed in the NiN₄/PMS system. Firstly, compared to CN, NiN₄ showed much lower charge transfer resistance (Fig. S29) and much higher current response in the PMS system (Fig. S30). The current response of NiN₄ was further increased when adding BPA into the system, indicating the enhanced charge transfer in the system. Moreover, the open-circuit potential (OCP) test is widely used to detect ETP directly.[29] As shown in Fig. 4b, the OCP was increased from ~0.4 V to 0.78 V after PMS addition, which could be attributed to the formation of NiN₄-PMS complexes (NiN₄-PMS*) and the formation of Ni(IV)-Oxo species that elevated the potential of NiN₄. The addition of BPA caused the potential decrease, which could be due to the ETP from BPA to the NiN₄-PMS*. [31] The result also indicated CN was almost inert to the PMS system, which could explain its neglectable activity in PMS activation. The addition of other organics also showed decreased OCPs to different extent (Fig. 4c). For example, the addition of PhOH caused the greatest decline, and followed by adding BPA, MB, RhB, and MO, which indicated that their oxidation should be dominated by an ETP. An inferior descending trend was obtained for TET, OTC, CTC, IBU and ATZ, which showed a weaker ETP. The addition of PNP showed the lowest decrease,

indicating the weakest ETP. Interestingly, there is a roughly linear relation between the OCP drops and ln(k_{obs}) of different benzene series (excluding ATZ, which is a triazine) with a R² value of 0.89 (Fig. 4d). In the ETP, organics are oxidized by releasing electrons through the carbon matrix of the catalyst and transfer to the NiN₄-PMS*. Therefore, the intrinsic property, e.g., electron-loss capacity, of organics may highly affect the ETP efficiency, which will be discussed later.

Moreover, the electron transfer between the target pollutants and the NiN₄-PMS* was further analyzed using a galvanic oxidation system (GOS, Fig. S31).[13] Significantly different current changes were detected when PMS and different contaminants were added to PMS cells and contaminant cells (Fig. 4e). In particular, these GOS-related current formation results were consistent with the OCP results, and also the oxidation of pollutants in GOS (Fig. S32), which further confirmed that ETP are dominated for the contaminants with faster degradation rates (e.g., PhOH, BPA, MB, RhB) in the NiN₄/PMS system. Similarly, a linear relationship was also observed between the initial current value and ln (k_{obs}) of different benzene series (excluding ATZ) with a R² value of 0.92 (Fig. 4f). Notably, although ATZ showed a lower ETP effect (smaller OCP drop and current value) than CTC in NiN₄/PMS system (Figs. 4c and 4e), its oxidation kinetics was much higher than CTC, suggesting ATZ could be predominantly oxidized by Ni(IV)-Oxo species via direct electron transfer.[14] So, these results preliminarily revealed benzene series roughly followed a linear relationship between their oxidation behaviors and their electrochemical properties through ETP.

3.6. Theoretical analysis of the interaction between NiN₄ and PMS

The molecular orbitals of CN and NiN₄ were calculated via DFT to determine their electronic properties. The result indicates a significant decrease in the gap of highest occupied molecular orbital (HOMO) and lowest unoccupied molecular orbital (LUMO) from 3.4 eV (CN) to 1.9 eV (NiN₄, Fig. S33a), which leads to a reduction in the energy needed for the electrons to escape from the catalyst surface. The density of states (DOS) of NiN₄, compared to CN, exhibits a sharp feature from single atom Ni contribution at energies close to HOMO (Fig. S33b), indicating the number of occupied states increases sharply supported by single-atom Ni contributed.[20] Therefore, the charge transfer in the bulk and on the surface of the NiN₄ is enhanced as verified by the electrochemical analysis (Figs. S29 and S30). The two-dimensional charge distribution image (Fig. S34) shows CN has a relatively uniform charge distribution, while the charge density of NiN₄ were modulated and located around Ni-N₄ sites, which could be attributed to the differences in valence electron and electronegativity of Ni, N, and C atoms.[31] The charge redistribution explains the highly activity of NiN₄ for PMS adsorption and activation because high electron density at Ni-N₄ sites can strongly attract electrophilic PMS molecules.[37] Also, corroborating with the active sites predicted by condensed dual descriptors (CDD) results (Fig. S35), it is further verified the essential role of Ni-N₄ sites in the NiN₄/PMS system as the Ni site has the highest CDD value. [38].

Fig. 5a showed the completely relaxed atomic configurations of the PMS with different O sites adsorbed on the Ni sites after geometry optimization, which indicates the model via adsorbing para-position O (mode A) should be the most likely adsorption conduct as its adsorption energy (E_{ads}) value was the most negative (-3.68 eV). However, it should be noticed that the other two models via adsorbing one peroxy oxygen in a middle mode (mode B) and terminal end-on mode (mode C) also show considerable negative E_{ads} of -3.13 and -2.78 eV, indicating that Ni sites of NiN₄ have strong PMS binding affinity and all these three models could co-exist in the NiN₄/PMS system. Under these three adsorption models (NiN₄-PMS*), significant electron transfer occurred between NiN₄ and PMS based on the charge density difference analysis (Fig. 5a).[39] Among them, model C shows that the charge transfer from the adsorbed PMS to NiN₄ reaches 1.2 e, suggesting it is the easiest transitional configuration to occur transformation.[40] The

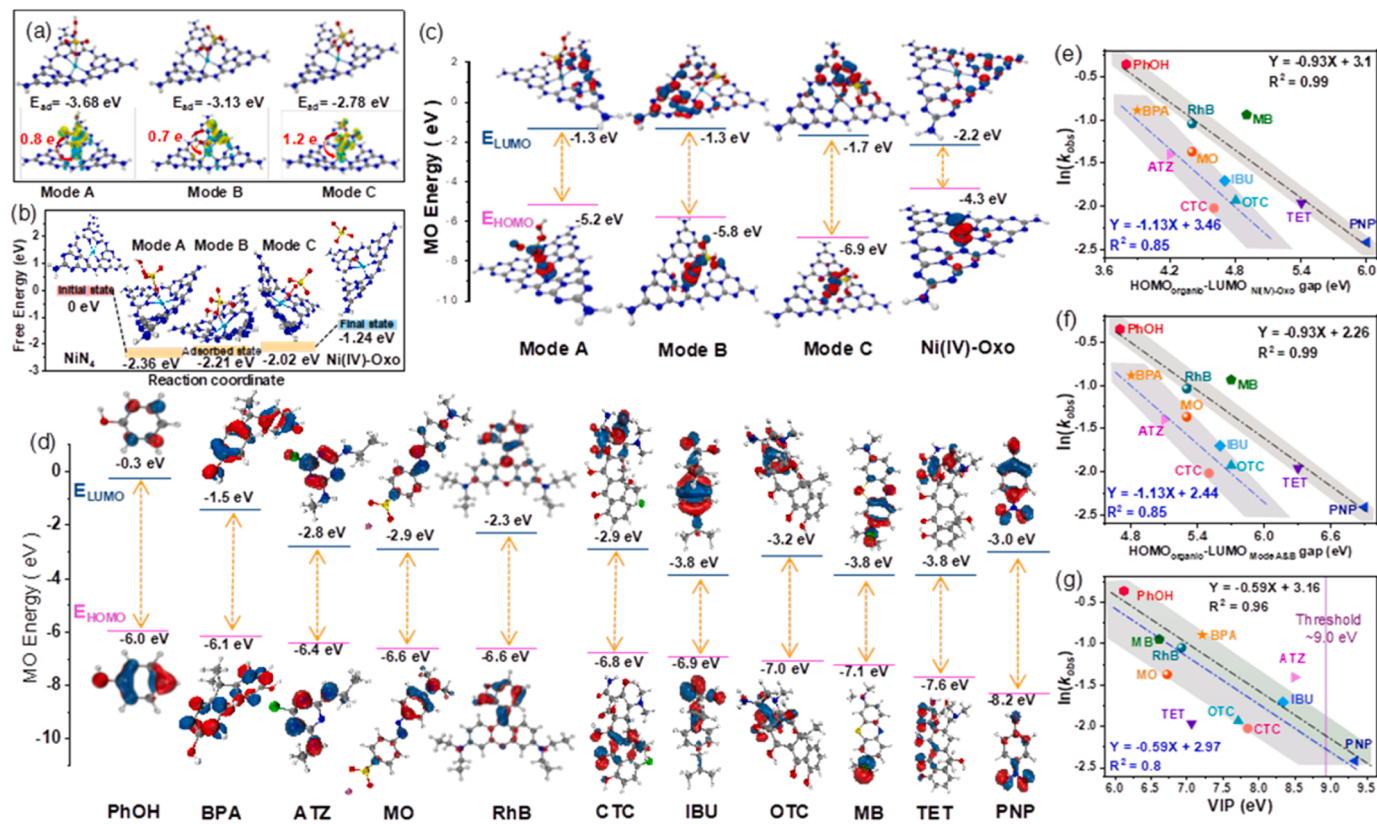


Fig. 5. (a) Optimized configurations and E_{ads} of different O sites for PMS adsorbed on Ni site of NiN_4 , and the calculated electron density difference diagrams (including electron transfer) of NiN_4 with PMS adsorbed on the Ni site (the yellow and cyan equivalence surfaces represent the regions of increasing and decreasing electron density, respectively). (b) Free energy changes against reaction pathways of PMS activation at Ni-N_4 sites. The HOMO and LOMO of (c) three kinds intermediate states and Ni(IV)-Oxo species, and (d) different model organic pollutants. Relationship between the (e) $\text{HOMO}_{\text{Organic}}-\text{LUMO}_{\text{Ni(IV)-Oxo}}$ gap, (f) $\text{HOMO}_{\text{Organic}}-\text{LUMO}_{\text{Model A\&B}}$ gap, or (g) VIP and $\ln(k_{\text{obs}})$ of pollutants. (Grey for C, dark blue for N, white for H, cyan for Ni, yellow for S, red for O, green for Cl, purple for Na).

adsorption complexes of NiN_4 -PMS show substantially reduced free energy of -2.36 , -2.21 and -2.02 eV for model A, B and C, respectively, when compared to the original state of NiN_4 (Fig. 5b). Based on the dissociation of the adsorbed PMS, Ni(IV)-Oxo species could be evolved.[21] As illustrated in Fig. 5b, the formation of Ni(IV)-Oxo species from intermediate mode C state affords the smallest energy barrier (0.78 eV). Combining with the charge transfer results (Fig. 5a), it can be speculated that mode C would be the most possible intermediate state to evolve Ni(IV)-Oxo in the NiN_4 /PMS system. Furthermore, although mode C has the most potential to evolve Ni(IV)-Oxo , model A and B with more negative E_{ads} would co-exist in the NiN_4 /PMS system as metastable species that could derive ETP.[13] This co-existed of NiN_4 -PMS* and also Ni(IV)-Oxo species should be ascribed to the modulated electronic structures of Ni-N_4 sites that stabilize the these intermediate species. Generally, these results indicate NiN_4 is highly active in adsorption and activation of PMS to form three kinds of NiN_4 -PMS* and also Ni(IV)-Oxo species, which explains the existence of both ETP and high-valent metal oxidation in the NiN_4 /PMS system.

3.7. Dual-pathway NRO in NiN_4 /PMS system

To further understand the selective oxidation of different organics, the HOMO and LUMO of three kinds of NiN_4 -PMS*, Ni(IV)-Oxo species, and all model organic pollutants were further analyzed. As depicted in Fig. 5c, the HOMO values are -5.2 , -5.8 , -6.9 and -4.3 eV, and the LUMO values are -1.3 , -1.3 , -1.7 and -2.2 eV for model A, B, C and Ni(IV)-Oxo species, respectively. The lowest LUMO of Ni(IV)-Oxo species suggests that the electrons from organic can transfer to it most easily due to the energy barrier for electron transfer to this orbital is the

smallest.[11,34] However, it should be also noted that the co-existed model A, B and C are also thermodynamically feasible species that could trigger ETP in the NiN_4 /PMS system. The HOMO distribution diagrams also reveal that electrons of organics could be easily transferred via the triazine ring of NiN_4 to adsorbed PMS or Ni(IV)-Oxo species, and organics with electron-rich conjugated systems, e.g., aromatic rings, would favor the interaction.[29].

As to the model pollutants, their HOMO (HOMO_{Organic}) were in the range of $-6.0 \sim -8.2$ eV (Fig. 5d). A narrow difference between the HOMO_{Organic} and the LUMO values of three kinds intermediate states and Ni(IV)-Oxo species could facilitate the charge transfer, suggesting organics with a narrow gap between them should be oxidized more easily due to the energy barriers are smaller.[41] As shown in Figs. 5e-5f, the $\ln(k_{\text{obs}})$ and the gap of HOMO_{Organic} and LUMO_{Ni(IV)-Oxo} or LUMO_{Model A&B} have roughly linear relationships and can be divided into two groups (excluding MB). As to PhOH, RhB, TET and PNP, they follow a linear relation with a R^2 of 0.99, and the fitting linear relation has a R^2 of 0.85 for BPA, ATZ, MO, IBU, CTC and OTC. Similarly, the $\ln(k_{\text{obs}})$ and the gap of HOMO_{Organic} and LUMO_{Model C} (Fig. S36a) or HOMO_{Organic} (Fig. S36b) also shows the same relationship. However, no obvious regular relationships were observed between $\ln(k_{\text{obs}})$ and LUMO_{Organic} (Fig. S37a) or HOMO-LOMO gap of organics (Fig. S37b). Therefore, the oxidation kinetics of organics can be roughly predicted by their HOMO values in the NiN_4 /PMS system.[42] Typically, the highest HOMO of PhOH enables it with the highest k_{obs} , while it is the lowest for PNP due to its lowest HOMO.

In addition to the HOMO of organics, vertical ionization potential (VIP) is also used to analyze the oxidation kinetics of pollutants. Generally, a higher VIP means more difficult to lose electrons.[29] The

calculated VIP values of the model organics (Table S4) and their relationship with $\ln(k_{obs})$ is exhibited in Fig. 5g. Interestingly, a strong linear relationship with R^2 of 0.96 is also observed for the group of PhOH, BPA, MB, RhB, IBU and PNP, and there is a linear relation with R^2 of 0.8 when further including MO, OTC and CTC, suggesting the oxidation kinetics of organic in the NiN_4/PMS system is roughly determined by its VIP value. It can be noticed that it is more suitable to evaluate the oxidation kinetics of MB and CTC by their VIP value (Fig. 5g), while ATZ and TET are more reasonable in using $\text{HOMO}_{\text{organic}}$ value (Figs. 5e-5f). Additionally, although MO and RhB has the same HOMO value of -6.6 eV, and MO has a smaller VIP value (6.72 eV) than RhB (6.92 eV), the cationic RhB has a higher oxidation rate than anionic MO, suggesting the electrostatic adsorption also affects the oxidation behavior of pollutants (RhB has a higher adsorption than MO on NiN_4 , Fig. S21). Furthermore, albeit the VIP value of PNP is higher than the threshold of 9.0 eV (an organic substrate with higher IP value than the threshold cannot serve as electron donor in the electron transfer process),^[43] it can be also oxidized effectively in the NiN_4/PMS system ($k_{obs} = 0.09 \text{ min}^{-1}$). When PNP is adsorbed by Ni(IV)-Oxo (post-optimized configuration, Fig. S38), the charge transfer from the adsorbed PNP to Ni(IV)-Oxo is 0.4 e, suggesting PNP can be oxidized by the highly oxidative Ni(IV)-Oxo species via direct electron transfer.^[34] However, it is difficult to distinguish the occupied oxidation mechanism for different organic compounds. As revealed by the scavenging experiments (Fig. 3g) and electrochemical tests (Figs. 4c and 4e), both ETP and Ni(IV)-Oxo oxidation contributed to the degradation of these model organics. Generally, both VIP and $\text{HOMO}_{\text{organic}}$ are important nature properties of organic in determining its oxidation behavior in the NiN_4/PMS system via nonradical oxidation in the presence of $\text{NiN}_4\text{-PMS}^*$ and Ni(IV)-Oxo species, and the high-valent Ni(IV)-Oxo species also served highly efficient oxidant to oxidize organics directly (Fig. 6).

4. Conclusion

SACs can be precisely engineered to exhibit high selectivity for specific contaminants, making them suitable for targeted pollutant removal. This selectivity minimizes the generation of harmful byproducts. This study demonstrated a novel dual-pathway NRO process in PMS activation via a new developed NiN_4 catalyst for highly efficient and selective removal of POPs. The Ni-N₄ sites were revealed as the reactive centers and exhibited strong interaction with PMS because of their highly modulated electronic structures, which derived both surface-bonding active complexes ($\text{NiN}_4\text{-PMS}^*$) and high-valent Ni(IV)-Oxo species. The metastable $\text{NiN}_4\text{-PMS}^*$ and Ni(IV)-Oxo species with

strong electron affinity resulted in highly selective oxidation towards pollutants. It was revealed that the oxidation behaviors of benzene series roughly followed a linear relationship with their electrochemical properties. Furthermore, the gap between $\text{HOMO}_{\text{organic}}$ and LOMO of metastable species, and VIP values of organics also determined the oxidation kinetics in the NiN_4/PMS system. Therefore, pollutants with a relatively high HOMO or relatively low VIP, were oxidized with high k_{obs} (e.g., ~ 0.70 and $\sim 0.41 \text{ min}^{-1}$ for PhOH and BPA, respectively). The highly oxidative Ni(IV)-Oxo species also enables effective degradation of organics with strong electron-withdrawing group organics, e.g., PNP (k_{obs} of 0.09 min^{-1}), in the NiN_4/PMS system. This $\text{NiN}_4\text{-PMS}^*$ and Ni(IV)-Oxo species dominated NRO rendered the applicability of NiN_4/PMS system in the presence of inorganic anions and natural organic matters, and over a wide pH range (3–10), and in real water matrixes. Combined with the excellent scalability of NiN_4 synthesis method (facile pyrolysis), the proposed NiN_4/PMS system showed great potential in industrial wastewater treatment. However, it should be noticed future research efforts would likely focus on improving the regeneration and longevity of NiN_4 to reduce operational costs and extend their service life in practical applications. Overall, based on the dual-pathway NRO process, the NiN_4/PMS system offered a promising avenue for efficient and selective contaminant removal with potential benefits in sustainability, resource utilization, and environmental impact reduction. Ongoing research and development in this field would lead to further advancements and practical applications in water treatment and environmental remediation.

Appendix A. Supporting information

Supplementary data associated with this article can be found in the online version at doi:

Analytical methods, electrochemical test, theoretical calculations, morphology of CN and NiN_4 , Ni loading amount, XRD, BET, XPS, two-dimensional LOL color-filled map, WT-EXAFS, HPLC-MS, possible degradation pathway of BPA, different oxidants, BPA degradation and k, effects of reaction temperature, pH, catalyst dosage, PMS concentration, inorganic ions, degradation of BPA with Cl^- in different systems, humic acid, different water backgrounds, stability tests, XRD and XPS of used catalyst, adsorption of various organics, quenching tests, relationship between the TOC removal ratio and $\ln(k_{obs})$ of pollutants, EPR results, effects of dissolved O_2 , effect of premixing time, PMS consumption, XANES spectra, EIS plots, LSV plots, GOS reaction device setup, removal ratios of different organics in the GOS, molecular orbital energies and structures, density of states, two-dimensional charge distribution image, CDD, relationship between the $\text{HOMO}_{\text{organic}} - \text{LUMO}_{\text{Model C}}$ gap, $\text{HOMO}_{\text{organic}}, \text{LUMO}_{\text{organic}}$ or HOMO-LUMO gap of organics and $\ln(k_{obs})$ of pollutants, charge density differences of the post-optimized structure of the adsorbed PNP on Ni(IV)-Oxo (PDF).

CRediT authorship contribution statement

Liu Yilin: Formal analysis. **Zeng Qingyi:** Conceptualization, Funding acquisition, Supervision, Writing – review & editing. **Duan Xiaoguang:** Conceptualization, Supervision, Writing – review & editing. **Xu Xing:** Formal analysis, Methodology. **Tan Jing:** Investigation. **Zhang Qingyan:** Investigation. **Zeng Qingming:** Formal analysis, Investigation, Writing – original draft. **Wen Yanjun:** Investigation.

Declaration of Competing Interest

The authors declare that they have no known competing financial interests or personal relationships that could have appeared to influence the work reported in this paper.

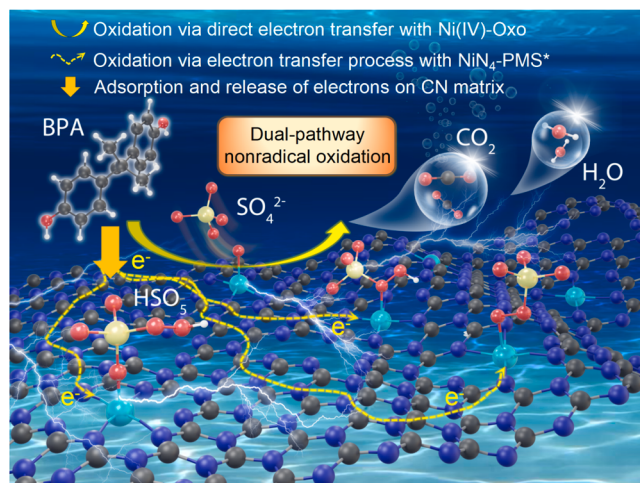


Fig. 6. Illustration of the dual-pathway NRO process in the NiN_4/PMS system for BPA degradation.

Data Availability

Data will be made available on request.

Acknowledgements

This work was supported by the National Natural Science Foundation of China (52170083, 51808143), the Hunan Provincial Natural Science Foundation of China (2021JJ20007), the Science and Technology Innovation Program of Hunan Province (2022RC1125). Q. Zeng acknowledges the State Scholarship Fund of China Scholarship Council Foundation (202008440212). The comments and advice from editor and anonymous reviewers are highly appreciated, which help greatly enhance the overall quality of the paper.

Appendix A. Supporting information

Supplementary data associated with this article can be found in the online version at [doi:10.1016/j.apcatb.2024.123752](https://doi.org/10.1016/j.apcatb.2024.123752).

References

- [1] K.C. Jones, Persistent organic pollutants (POPs) and related chemicals in the global environment: some personal reflections, Environ. Sci. Technol. 55 (2021) 9400–9412, <https://doi.org/10.1021/acs.est.0c08093>.
- [2] J. Ma, H. Hung, C. Tian, R. Kallenborn, Revolatilization of persistent organic pollutants in the Arctic induced by climate change, Nat. Clim. Chang 1 (2011) 255–260, <https://doi.org/10.1038/nclimate1167>.
- [3] W.-W. Li, H.-Q. Yu, B.E. Rittmann, Chemistry: reuse water pollutants, Nature 528 (2015) 29–31, <https://doi.org/10.1038/528029a>.
- [4] X. Yu, H. Liu, Y. Huang, C. Li, L. Kuang, J. Zhong, S. Zhu, Y. Gou, Y. Wang, Y. Zhang, G. Shan, Z. Lv, S. Zhang, L. Zhu, A green edge-hosted zinc single-site heterogeneous catalyst for superior Fenton-like activity, Proc. Nat. Acad. Sci. 120 (2023) e2221228120, <https://doi.org/10.1073/pnas.2221228120>.
- [5] M. Yang, K. Wu, S. Sun, J. Duan, X. Liu, J. Cui, S. Liang, Y. Ren, Unprecedented relay catalysis of curved Fe₁–N₄ single-atom site for remarkably efficient ¹O₂ generation, ACS Catal. 13 (2023) 681–691, <https://doi.org/10.1021/acs.catal.2c05409>.
- [6] W. Li, L. Jin, S. Jiang, Y. Liu, Electrified nitrogen-doped mxene membrane electrode for micropollutants decontamination via peroxymonosulfate activation, ACS EST Eng. (2023), <https://doi.org/10.1021/acs.estengg.3c00222>.
- [7] Y. Gao, Y. Zhou, S.-Y. Pang, J. Jiang, Y.-M. Shen, Y. Song, J.-B. Duan, Q. Guo, Enhanced peroxymonosulfate activation via complexed Mn(II): A novel non-radical oxidation mechanism involving manganese intermediates, Water Res 193 (2021) 116856, <https://doi.org/10.1016/j.watres.2021.116856>.
- [8] Y. Gao, Y. Zhu, Z. Chen, C. Hu, Nitrogen-coordinated cobalt embedded in a hollow carbon polyhedron for superior catalytic oxidation of organic contaminants with peroxymonosulfate, ACS EST Eng. 1 (2021) 76–85, <https://doi.org/10.1021/acs.estengg.0c00039>.
- [9] J.E. Grebel, J.J. Pignatello, W.A. Mitch, Effect of halide ions and carbonates on organic contaminant degradation by hydroxyl radical-based advanced oxidation processes in saline waters, Environ. Sci. Technol. 44 (2010) 6822–6828, <https://doi.org/10.1021/es1010225>.
- [10] P. Hu, M. Long, Cobalt-catalyzed sulfate radical-based advanced oxidation: a review on heterogeneous catalysts and applications, Appl. Catal. B 181 (2016) 103–117, <https://doi.org/10.1016/j.apcatb.2015.07.024>.
- [11] P. Cai, X. Zhang, S. Yang, H. Cui, Y. Wang, Y. Huang, M. Qin, D. Han, X. Yang, P. Guo, Y. Sun, D. Yang, NiCo₂N nanosheets catalyzed peroxymonosulfate activation to generate ¹O₂ and SO₄²⁻ for efficient pollutant degradation: The role of nitrogen atoms, Appl. Catal. B 342 (2024), <https://doi.org/10.1016/j.apcatb.2023.123446>.
- [12] J. Miao, Y. Zhu, J. Lang, J. Zhang, S. Cheng, B. Zhou, L. Zhang, P.J.J. Alvarez, M. Long, Spin-state-dependent peroxymonosulfate activation of single-atom M–N moieties via a radical-free pathway, ACS Catal. 11 (2021) 9569–9577, <https://doi.org/10.1021/acscatal.1c02031>.
- [13] Y. Qi, J. Li, Y. Zhang, Q. Cao, Y. Si, Z. Wu, M. Akram, X. Xu, Novel lignin-based single atom catalysts as peroxymonosulfate activator for pollutants degradation: Role of single cobalt and electron transfer pathway, Appl. Catal. B 286 (2021) 119910, <https://doi.org/10.1016/j.apcatb.2021.119910>.
- [14] J. Jiang, Z. Zhao, J. Gao, T. Li, M. Li, D. Zhou, S. Dong, Nitrogen vacancy-modulated peroxymonosulfate nonradical activation for organic contaminant removal via high-valent cobalt-oxo species, Environ. Sci. Technol. 56 (2022) 5611–5619, <https://doi.org/10.1021/acs.est.2c01913>.
- [15] O. Pestovsky, A. Bakac, Reactivity of aqueous Fe(IV) in hydride and hydrogen atom transfer reactions, J. Am. Chem. Soc. 126 (2004) 13757–13764, <https://doi.org/10.1021/ja0457112>.
- [16] M.K. Kuimova, G. Yahiroglu, P.R. Ogilby, Singlet oxygen in a cell: spatially dependent lifetimes and quenching rate constants, J. Am. Chem. Soc. 131 (2009) 332–340, <https://doi.org/10.1021/ja807484b>.
- [17] Z. Wang, W. Qiu, S. Pang, Q. Guo, C. Guan, J. Jiang, Aqueous Iron(IV)-oxo complex: an emerging powerful reactive oxidant formed by iron(II)-based advanced oxidation processes for oxidative water treatment, Environ. Sci. Technol. 56 (2022) 1492–1509, <https://doi.org/10.1021/acs.est.1c04530>.
- [18] Z. Zhao, P. Zhang, H. Tan, X. Liang, T. Li, Y. Gao, C. Hu, Low concentration of peroxymonosulfate triggers dissolved oxygen conversion over single atomic Fe–N₃O₁ sites for water decontamination, Small 19 (2023) 2205583, <https://doi.org/10.1002/smll.202205583>.
- [19] C. Yang, S. Shang, Y. Fan, K. Shih, X. Li, L. Lin, Incorporation of atomically dispersed cobalt in the 2D metal–organic framework of a lamellar membrane for highly efficient peroxymonosulfate activation, Appl. Catal. B 325 (2023) 122344, <https://doi.org/10.1016/j.apcatb.2022.122344>.
- [20] L.-S. Zhang, X.-H. Jiang, Z.-A. Zhong, L. Tian, Q. Sun, Y.-T. Cui, X. Lu, J.-P. Zou, S.-L. Luo, Carbon nitride supported high-loading fe single-atom catalyst for activation of peroxymonosulfate to generate ¹O₂ with 100% Selectivity, Angew. Chem. Int Ed. 60 (2021) 21751–21755, <https://doi.org/10.1002/anie.202109488>.
- [21] J. Miao, J. Song, J. Lang, Y. Zhu, J. Dai, Y. Wei, M. Long, Z. Shao, B. Zhou, P.J. J. Alvarez, L. Zhang, Single-atom MnN₅ catalytic sites enable efficient peroxymonosulfate activation by forming highly reactive Mn(IV)-oxo species, Environ. Sci. Technol. 57 (2023) 4266–4275, <https://doi.org/10.1021/acs.est.2c08836>.
- [22] Y. Zheng, Y. Jiao, Y. Zhu, Q. Cai, A. Vasileff, L.H. Li, Y. Han, Y. Chen, S.-Z. Qiao, Molecule-level g-C₃N₄ coordinated transition metals as a new class of electrocatalysts for oxygen electrode reactions, J. Am. Chem. Soc. 139 (2017) 3336–3339, <https://doi.org/10.1021/jacs.6b13100>.
- [23] H. Li, C. Shan, B. Pan, Fe(III)-doped g-C₃N₄ mediated peroxymonosulfate activation for selective degradation of phenolic compounds via high-valent iron-oxo species, Environ. Sci. Technol. 52 (2018) 2197–2205, <https://doi.org/10.1021/acs.est.7b05563>.
- [24] J. Liu, Z. Liu, H. Wang, B. Liu, N. Zhao, C. Zhong, W. Hu, Designing nanoporous coral-like Pt nanowires architecture for methanol and ammonia oxidation reactions, Adv. Funct. Mater. 32 (2022) 2110702, <https://doi.org/10.1002/adfm.202110702>.
- [25] L. Cheng, H. Yin, C. Cai, J. Fan, Q. Xiang, Single Ni atoms anchored on porous few-layer g-C₃N₄ for photocatalytic CO₂ reduction: the role of edge confinement, Small 16 (2020) 2002411, <https://doi.org/10.1002/smll.202002411>.
- [26] X. Shi, Y. Huang, Y. Bo, D. Duan, Z. Wang, J. Cao, G. Zhu, W. Ho, L. Wang, T. Huang, Y. Xiong, Highly selective photocatalytic CO₂ methanation with water vapor on single-atom platinum-decorated defective carbon nitride, Angew. Chem. Int. Ed. 61 (2022) e202203063, <https://doi.org/10.1002/anie.202203063>.
- [27] Y. Lu, H. Wang, P. Yu, Y. Yuan, R. Shahbazian-Yassar, Y. Sheng, S. Wu, W. Tu, G. Liu, M. Kraft, R. Xu, Isolated Ni single atoms in nitrogen doped ultrathin porous carbon templated from porous g-C₃N₄ for high-performance CO₂ reduction, Nano Energy 77 (2020) 105158, <https://doi.org/10.1016/j.nanoen.2020.105158>.
- [28] X. Chen, F.O. Guddha, X. Hu, M.G. Waigi, Y. Gao, Degradation of bisphenol A in an oxidation system constructed from Mo₂C MXene and peroxymonosulfate, NPJ Clean. Water 5 (2022) 66, <https://doi.org/10.1038/s41545-022-00214-w>.
- [29] K. Yin, Y. Shang, D. Chen, B. Gao, Q. Yue, X. Xu, Redox potentials of pollutants determining the dominate oxidation pathways in manganese single-atom catalyst (Mn-SAC)/peroxymonosulfate system: Selective catalytic mechanisms for versatile pollutants, Appl. Catal. B 338 (2023) 123029, <https://doi.org/10.1016/j.apcatb.2023.123029>.
- [30] J. Li, M. Li, H. Sun, Z. Ao, S. Wang, S. Liu, Understanding of the oxidation behavior of benzyl alcohol by peroxymonosulfate via carbon nanotubes activation, ACS Catal. 10 (2020) 3516–3525, <https://doi.org/10.1021/acscatal.9b05273>.
- [31] M. Yang, Z. Hou, X. Zhang, B. Gao, Y. Li, Y. Shang, Q. Yue, X. Duan, X. Xu, Unveiling the origins of selective oxidation in single-atom catalysis via Co–N₄–C intensified radical and nonradical pathways, Environ. Sci. Technol. 56 (2022) 11635–11645, <https://doi.org/10.1021/acs.est.2c01261>.
- [32] J. Qi, J. Liu, F. Sun, T. Huang, J. Duan, W. Liu, High active amorphous Co(OH)₂ nanocages as peroxymonosulfate activator for boosting acetaminophen degradation and DFT calculation, Chin. Chem. Lett. 32 (2021) 1814–1818, <https://doi.org/10.1016/j.cclet.2020.11.026>.
- [33] S. Liu, Z. Zhang, F. Huang, Y. Liu, L. Feng, J. Jiang, L. Zhang, F. Qi, C. Liu, Carbonized polyaniline activated peroxymonosulfate (PMS) for phenol degradation: Role of PMS adsorption and singlet oxygen generation, Appl. Catal. B 286 (2021) 119921, <https://doi.org/10.1016/j.apcatb.2021.119921>.
- [34] Z. Wang, W. Wang, J. Wang, Y. Yuan, Q. Wu, H. Hu, High-valent iron-oxo species mediated cyclic oxidation through single-atom Fe-N₆ sites with high peroxymonosulfate utilization rate, Appl. Catal. B 305 (2022) 121049, <https://doi.org/10.1016/j.apcatb.2021.121049>.
- [35] S. Park, K. Jin, H.K. Lim, J. Kim, K.H. Cho, S. Choi, H. Seo, M.Y. Lee, Y.H. Lee, S. Yoon, M. Kim, H. Kim, S.H. Kim, K.T. Nam, Spectroscopic capture of a low-spin Mn(IV)-oxo species in Ni–Mn₂O₄ nanoparticles during water oxidation catalysis, Nat. Commun. 11 (2020) 5230, <https://doi.org/10.1038/s41467-020-19133-w>.
- [36] D.H. Pearson, C.C. Ahn, B. Fultz, White lines and d-electron occupancies for the 3d and 4d transition metals, Phys. Rev. B 47 (1993) 8471–8478, <https://doi.org/10.1103/PhysRevB.47.8471>.
- [37] Q. Zhou, C. Song, P. Wang, Z. Zhao, Y. Li, S. Zhan, Generating dual-active species by triple-atom sites through peroxymonosulfate activation for treating micropollutants in complex water, Proc. Nat. Acad. Sci. 120 (2023) e2300085120, <https://doi.org/10.1073/pnas.2300085120>.
- [38] Y. Sun, H. Li, S. Zhang, M. Hu, J. Qian, B. Pan, Revisiting the heterogeneous peroxymonosulfate activation by MoS₂: A surface Mo-peroxymonosulfate complex as the major reactive species, ACS EST Water 2 (2022) 376–384, <https://doi.org/10.1021/acsestwater.1c00459>.

[39] Y. Gao, T. Wu, C. Yang, C. Ma, Z. Zhao, Z. Wu, S. Cao, W. Geng, Y. Wang, Y. Yao, Y. Zhang, C. Cheng, Activity trends and mechanisms in peroxyomonosulfate-assisted catalytic production of singlet oxygen over atomic metal-N-C catalysts, *Angew. Chem. Int. Ed.* 60 (2021) 22513–22521, <https://doi.org/10.1002/anie.202109530>.

[40] Y. Gao, Y. Zhu, L. Lyu, Q. Zeng, X. Xing, C. Hu, Electronic structure modulation of graphitic carbon nitride by oxygen doping for enhanced catalytic degradation of organic pollutants through peroxyomonosulfate activation, *Environ. Sci. Technol.* 52 (2018) 14371–14380, <https://doi.org/10.1021/acs.est.8b05246>.

[41] X. Liu, H. Yu, J. Ji, Z. Chen, M. Ran, J. Zhang, M. Xing, Graphene oxide-supported three-dimensional cobalt–nickel bimetallic sponge-mediated peroxyomonosulfate activation for phenol degradation, *ACS EST Eng.* 1 (2021) 1705–1714, <https://doi.org/10.1021/acsestengg.1c00307>.

[42] S. Wang, J. Kang, P. Yan, J. Shen, J. Zuo, Y. Cheng, L. Shen, B. Wang, S. Zhao, Z. Chen, Surface oxygen vacancy enhanced the activation of peroxyomonosulfate on $\alpha\text{-Ni}_{0.2}\text{Fe}_{1.8}\text{O}_3$ for water decontamination: The overlooked role of H_2O in interface mechanism, *Appl. Catal. B* 342 (2024) 123419, <https://doi.org/10.1016/j.apcatb.2023.123419>.

[43] Z. Wang, Y. Wang, W. Wang, D. Wu, Q. Wu, H. Hu, Highly selective production of singlet oxygen by manipulating the spin state of single-atom Co–N moieties and electron localization, *Appl. Catal. B* 324 (2023) 122248, <https://doi.org/10.1016/j.apcatb.2022.122248>.